H, 4.33; N, 2.19. Found: C, 52.71; H, 4.42; N, 2.26.

***trans,trans*-[(dpe)$_2$MoF(NN=CMeCH$_2$CH$_2$CMe=NN)MoF(dpe)$_2$][BF$_4$]$_2$·2(CH$_2$Cl$_2$) (14c·2(CH$_2$Cl$_2$))**: greenish brown crystals. ^{1}H NMR (CDCl$_3$) δ -0.17 (s, 6 H, Me), 1.64 (s, 4 H, NN=CCH$_2$), 2.7-2.9 (m, 8 H, CH$_2$ of dpe), 2.9-3.1 (m, 8 H, CH$_2$ of dpe), 6.8-7.5 (m, 80 H, Ph); IR 1570 cm^{-1} (C=N). Anal. Calcd for $C_{112}H_{110}N_4Mo_2Cl_4P_8F_{10}B_2$: C, 58.36; H, 4.81; N, 2.43. Found: C, 57.92; H, 4.94; N, 2.46.

***trans,trans*-[(dpe)$_2$MoF(NN=CHCHMeCHMeCH=NN)MoF(dpe)$_2$][BF$_4$]$_2$·CH$_2$Cl$_2$ (14d·CH$_2$Cl$_2$)**: greenish brown crystals. ^{1}H NMR (CDCl$_3$) δ (*threo*-isomer) -0.02 (d, J = 7.0 Hz, 6 H, Me), 1.55 (m, 2 H, CHMe), 5.88 (d, J = 2.8 Hz, 2 H, NN=CH), (*erythro*-isomer) 0.06 (d, J = 6.1 Hz, 6 H, Me), 1.25 (m, 2 H, CHMe), 5.94 (d, J = 4.6 Hz, 2 H, NN=CH), 2.6-3.0 (m, 16 H, CH$_2$ of dpe), 6.8-7.5 (m, 80 H, Ph); IR 1567 cm^{-1} (C=N). Anal. Calcd for $C_{111}H_{108}N_4Mo_2Cl_2P_8F_{10}B_2$: C, 60.04; H, 4.90; N, 2.52. Found: C, 60.32; H, 5.03; N, 2.57.

Collection of Diffraction Data and Structure Refinements. Diffraction data were collected on Rigaku AFC-6A (for **2f**·C$_6$H$_6$ and **7a** at The Kanagawa University) and Rigaku AFC-5 (for *threo*-**14b**·6(C$_6$H$_6$) at The University of Tokyo) four-cycle automated diffractometers with Mo Kα (λ = 0.7107 Å) radiation and a graphite monochromator. In each case, crystal sealed in a glass capillary under argon was used, and data were collected at room temperature. Empirical absorption and Lorentz-polarization corrections were made. Selected crystallographic data are summarized in Table VII.

Structure solution and refinement were performed by using the UNIX-III program at the computer center of The University of Tokyo.[27] Tungsten atoms in the asymmetric units were found by the direct-methods program MULTAN or SHELXS86. Subsequent block-diagonal least-squares refinement and difference Fourier maps revealed all non-hydrogen atoms, which were refined by using anisotropic temperature factors taken from ref 28. The hydrogen atoms of **2f**·C$_6$H$_6$ and **7a** except for the NH hydrogens of **7a** were placed at the calculated positions and included in the final stage of refinement with isotropic thermal parameters. The hydrogens of *threo*-**14b**·6(C$_6$H$_6$) and the NH hydrogens of **7a** were not included in the structure refinement. The absolute structure of complex **7a** in the crystal was determined based on the anomalous dispersion effects. In the structure refinement of *threo*-**14b**·6(C$_6$H$_6$), difference Fourier maps showed six peaks of comparable electron density assignable to F atoms in a BF_4^- anion. These six peaks were refined as disordered F atoms with an atom multiplicity of 0.67. The difference maps also suggested that the positions of C(2) and C(3) are disordered to a minor extent, and this is probably the reason why the bond lengths and angles concerning these atoms include unusual values. An attempt to refine the minor disordered form was unsuccessful. The most intense residual peaks in the final difference Fourier maps are as follows: **2f**·C$_6$H$_6$, 0.89 e/Å^3, close to a P(2) atom; **7a**, 2.16 e/Å^3, close to a tungsten atom; *threo*-**14b**·6(C$_6$H$_6$), 3.20 e/Å^3, close to a tungsten atom.

Acknowledgment. This work was supported by the Ministry of Education of Japan and the Asahi Glass Foundation of Engineering Technology. We thank Professor Yosio Koike and Mr. Yuuki Abe of The Kanagawa University for the permission to use an X-ray diffractometer and experimental assistance.

Supplementary Material Available: Tables of positional parameters, anisotropic thermal parameters, bond lengths and angles for **2f**·C$_6$H$_6$, **7a**, and *threo*-**14b**·6(C$_6$H$_6$) (23 pages); tables of observed and calculated structure factors for **2f**·C$_6$H$_6$, **7a**, and *threo*-**14b**·6(C$_6$H$_6$) (118 pages). Ordering information is given on any current masthead page.

(27) Sakurai, T.; Kobayashi, K. *Rikagaku Kenkyusho Hokoku* **1979**, *55*, 69.

(28) International Tables for X-ray Crystallography; Kynoch Press: Birmingham, U.K., 1976; Vol. 3.

Electronic Structure of Paramagnetic Clusters of Transition Metal Ions. 2. Crystal and Molecular Structure, Single Crystal EPR Spectra, and Magnetic Properties of $[Co_6(\mu_3\text{-}S)_8(PEt_3)_6](PF_6)$

Alessandro Bencini,*,† Carlo A. Ghilardi,‡ Annabella Orlandini,‡ Stefano Midollini,‡ and Claudia Zanchini†

Contribution from the Dipartimento di Chimica, Università di Firenze and Istituto per lo Studio della Stereochimica ed Energetica dei Composti di Coordinazione, C.N.R., Firenze, Italy.
Received March 5, 1992

Abstract: The X-ray crystal structure of $[Co_6(\mu_3\text{-}S)_8(PEt_3)_6](PF_6)$ (PEt_3 = triethylphosphine) has shown that the crystals are rhombohedric, space group $R\bar{3}$, with a = 11.713 (6) Å, α = 92.15 (4)°, and isomorphous to the homologous iron cluster. The cluster possesses one unpaired electron, and its electronic structure has been investigated through UV-visible electronic absorption spectra, magnetic susceptibility measurements in the temperature range 4.2-300 K, and fluid and frozen solution and single-crystal EPR spectra. The experimental data have been rationalized using semiempirical models (ligand field and extended Hückel) and SCF-Xα-SW calculations. A comparison with the EPR spectra of the parent triclinic cluster $[Co_6(\mu_3\text{-}S)_8(PEt_3)_6](BPh_4)$ is carried out.

Introduction

Paramagnetic oligonuclear complexes of transition metals have been known for a long time, and although they are probably less numerous than diamagnetic complexes, their electronic structure has attracted the attention of researchers since the complexity of the spin structure and peculiar magnetic phenomena have always been considered a challenge to both theoreticians and experimentalists.[1-6] One of the best-known examples is copper(II) acetate hydrate, whose dinuclear nature was first recognized by Bleaney and Bowers in 1952 using EPR spectroscopy.[6] Chemists have synthesized a lot of compounds containing different metal atoms in the same molecule,[7] and also molecules in which the metal

† Dipartimento di Chimica, Università degli Studi di Firenze, Italy.
‡ I.S.S.E.C.C., C.N.R., Firenze, Italy.

(1) Martin, R. L. In *New Pathways in Inorganic Chemistry*; Ebsworth, E. A. V., Maddock, A. G., Sharpe, A. G., Eds.; Cambridge University Press: Cambridge, UK, 1968.
(2) Hodgson, D. J. *Prog. Inorg. Chem.* **1975**, *19*, 173.
(3) Cairns, C. J.; Bush, D. H. *Coord. Chem. Rev.* **1986**, *69*, 1.
(4) Kahn, O. *Struct. Bonding (Berlin)* **1987**, *68*, 89.
(5) Blondin, G.; Girered, J.-J. *Chem. Rev.* **1990**, *90*, 1359.
(6) Bleaney, B.; Bowers, K. D. *Proc. R. Soc.* **1952**, *A214*, 451.

0002-7863/92/1514-9898$03.00/0

atoms have non-integer oxidation states (the so-called "mixed valence" complexes).[8] The bonding and/or magnetic interactions can also extend through space, giving rise to solids with unusual physical and chemical properties.[9]

The theoretical treatment of this wide variety of compounds cannot generally be performed using a unified theory, especially when the magnetic structure, which requires theoretical methods accounting for electron correlation, is concerned. While a phenomenological description of the exchange interactions can usually be achieved using a spin hamiltonian approach,[10] a reasonable quantitative explanation of the magnetic properties of dinuclear and some tri- and tetranuclear complexes has been obtained using the Slater-Xα statistical approximation of the interelectronic interaction,[11] and structural–magnetic correlations have been established with the help of extended Hückel type calculations.[12,13]

In a number of cases most of the subtleties of the spin hamiltonian formalism have been exploited and compared to the available experimental (magnetic, Mössbauer, EPR) data.[10] When systems having non-integer oxidation states are considered, the complexity increases and the spin hamiltonian models require, generally, a number of parameters larger than the experimental data as soon as the nuclearity is larger than 2, and, up to now, the interpretation of their electronic structure is approached with simplified hamiltonians.[6,14,15] The most common approximations require higher symmetry spin structure than the actual ones, neglect of single ion zero field splitting effects, and a reduced number, even zero, of electron delocalization parameters.

Oligonuclear complexes of transition metal ions are in between the molecular systems and the extended solids and have been considered the linkage between molecular and solid-state chemistry.[16] They generally have a number of stable oxidation states larger than those found in smaller molecular compounds, but electronic interactions still localized within the cluster of metals. These compounds, therefore, cannot have the peculiar magnetic or charge transport phenomena observed in extended solids, but they can be a relevance in catalytic or electron transfer systems. From a theoretical point of view one can still hope to be able to treat their electronic structure with the quantum mechanical models used for molecules, avoiding the further approximations needed to treat extended solids.[17-20]

Since on increasing the nuclearity of the systems a larger number of experimental data would be necessary even to phenomenologically interpret their magnetic structure, in order to make a first attempt in this direction one has to look for systems with the as low as possible number of unpaired electrons in order to simplify as much as possible the magnetic parameters and their electronic description. The results of these investigations will hopefully constitute the building blocks of a theoretical investigation which would lead to the understanding of the magnetic and electronic structure of more complicated systems.

Among oligonuclear clusters, those derived from a general core M_6X_8, whose structure can be described by an octahedron of M atoms encased in a cube of X atoms (X = chalcogens, halogens), have attracted the interest of chemists as molecular models of the Chevrel phases of molybdenum chalcogenides which include high-temperature and high-field superconductors.[21-25] Their structure has been extensively studied, and efforts have been made to synthesize molecular models which allow the study of the molecular structure of the constituent clusters, avoiding as much as possible solid-state interactions. Only very recently have the synthesis and structure of molecules with the formula $[Mo_6(\mu_3\text{-}S)_8(PEt_3)_6]^{0,1-}$ been reported.[26,27]

Table I. Crystallographic Data for $[Co_6(\mu_3\text{-}S)_8(PEt_3)_6](PF_6)$

compd	$C_{36}H_{90}Co_6F_6P_7S_8$	space group	$R\bar{3}$
fw	1464.04	λ(Mo Kα)	0.7107
a, Å	11.713 (6)	ρ_{calcd}, g cm^{-3}	1.516
α, deg	92.15 (4)	μ(Mo Kα), cm^{-1}	19.8
V, Å^3	1603.48	R	0.029
Z	1	R_w	0.029

With the aim of characterizing the molecular and electronic structure of "isolated" $[M_6S_8]^{n+}$ moieties, having an electronic system as simple as possible, we focused our attention on a series of complexes of general formula $[Co_6(\mu_3\text{-}S)_8(PEt_3)_6]^{n+}$, whose chemical synthesis and electrochemical behavior was previously reported.[28] Although clusters with n = 0, 1, and 2 have been electrochemically found to have comparable stabilities, only molecules with n = 0 and 1 have been isolated in the solid state. The n = 1 ion is paramagnetic with one unpaired electron, while the n = 0 cluster is diamagnetic. We have already measured the temperature dependence of the magnetic susceptibility and the single-crystal and solution EPR spectra of the complex $[Co_6(\mu_3\text{-}S)_8(PEt_3)_6](BPh_4)$, which possesses a $S = {}^1/_2$ ground state. Single-crystal EPR spectroscopy has shown a temperature dependence of the localization of the unpaired electron on the cobalt centers and the existence of feeble, but observable, magnetic interactions between the magnetic clusters.[29]

In order to have a higher symmetry complex and to investigate the effect of the chemical nature of the anion on the intra- and intercluster interactions, we have synthesized[28] the complex $[Co_6(\mu_3\text{-}S)_8(PEt_3)_6](PF_6)$, which is isomorphous[30] to $[Fe_6(\mu_3\text{-}S)_8(PEt_3)_6](PF_6)$, space group $R\bar{3}$, and we report here its crystal and molecular structure, magnetic properties, and single-crystal EPR spectra. For the description of the magnetic structure of the complex we will use a spin hamiltonian approach and parametrize the delocalization of the unpaired electron on the whole cluster using the delocalization parameter p. Since these systems contain only one unpaired electron we applied molecular orbital theories in order to have a qualitative and quantitative description of the various aspects of their chemistry. In particular we used extended Hückel results to qualitatively justify the nature of the ground state observed in the low-temperature EPR spectra and performed Xα-SW calculations in order to give an account as complete as possible of the observed spectroscopic properties and relative stabilities of the clusters.

Experimental Section

Synthesis of the Complex. The complex $[Co_6(\mu_3\text{-}S)_8(PEt_3)_6](PF_6)$ was prepared following the procedure previously described.[28] Single crystals suitable for X-ray analysis were obtained directly from the synthetic

(7) *Magneto-Structural Correlations in Exchange Coupled Systems*; Willett, R. D., Gatteschi, D., Kahn, O., Eds.; D. Riedel: Dordrecht, Holland, 1985.
(8) *Mixed Valence Compounds*; Brown, D. B., Ed.; D. Riedel: Dordrecht, Holland, 1980.
(9) *Electron Transfer in Biology and the Solid State*; Johnson, M. K., King, R. B., Kurtz, D. M., Kutal, C., Norton, M. L., Scott, R. A., Eds.; American Chemical Society: Washington, 1990; ACS Symp. Ser. No. 226.
(10) Bencini, A.; Gatteschi, D. *Electron Paramagnetic Resonance of Exchange Coupled Systems*; Springer Verlag: Berlin, 1990.
(11) Bencini, A. *J. Chim. Phys.* **1989**, *86*, 763.
(12) Hay, P. J.; Thibeault, J. C.; Hoffmann, R. *J. Am. Chem. Soc.* **1975**, *97*, 4884.
(13) Barbaro, P.; Bencini, A.; Bertini, I.; Briganti, F.; Midollini, S. *J. Am. Chem. Soc.* **1990**, *112*, 7238.
(14) Noodleman, L. *Inorg. Chem.* **1991**, *30*, 246.
(15) Noodleman, L. *Inorg. Chem.* **1991**, *30*, 256.
(16) Lee, S. C.; Holm, R. H. *Angew. Chem., Int. Ed. Engl.* **1990**, *29*, 840.
(17) Burdett, J. K.; Miller, G. J. *J. Am. Chem. Soc.* **1987**, *109*, 4081.
(18) Hoffman, G. G.; Bashkin, J. K.; Karplus, M. *J. Am. Chem. Soc.* **1990**, *112*, 8705.
(19) Wheeler, R. A. *J. Am. Chem. Soc.* **1990**, *112*, 8737.
(20) Albright, T. A.; Burdett, J. K.; Wahngbo, M. H. *Orbital Interactions in Chemistry*; John Wiley & Sons: New York, 1985.
(21) Chevrel, R.; Sergent, M.; Prigent, J. *Solid State Chem.* **1971**, *3*, 515.
(22) Fisher, O. *Appl. Phys.* **1978**, *16*, 1.
(23) Chevrel, R. *Superconductor Material Science: Metallurgy, Fabrication and Applications*; Foner, S., Schwartz, B. B., Eds.; Plenum Press: New York, 1981.
(24) Hughbanks, T.; Hoffmann, R. *J. Am. Chem. Soc.* **1983**, *105*, 1150.
(25) *Superconductivity in Ternary Compounds*; Fisher, O., Maple, M. B., Eds.; Springer-Verlag, Berlin, 1982; Vol. I.
(26) Saito, T.; Yamamoto, N.; Yamagata, T.; Imoto, H. *J. Am. Chem. Soc.* **1988**, *110*, 1646.
(27) Saito, T.; Yamamoto, N.; Nagase, T.; Tsuboi, T.; Kobayashi, K.; Yamagata, T.; Imoto, H.; Unoura, K. *Inorg. Chem.* **1990**, *29*, 764.
(28) Cecconi, F.; Ghilardi, C. A.; Midollini, S.; Orlandini, A.; Zanello, P. *Polyhedron* **1986**, *5*, 2021.
(29) Bencini, A.; Midollini, S.; Zanchini, C. *Inorg. Chem.* **1992**, *31*, 2132.
(30) Cecconi, F.; Ghilardi, C. A.; Midollini, S.; Orlandini, A.; Zanello, P. *J. Chem. Soc., Dalton Trans.* **1987**, 831.

procedure. Single crystals suitable for EPR spectroscopy were grown from a dichloromethane–*n*-butanol solution, by slow evaporation of the solvent.

X-ray Data Collection and Reduction. A black rhombohedron of approximate dimension 0.15 × 0.17 × 0.22 mm was mounted on a ENRAF NONIUS CAD4 automatic diffractometer. Unit cell dimensions were determined from a least-squares refinement of the angular settings of 25 carefully centered reflections. Crystal data are given in Table I. Intensity data within $2\theta \leq 50°$ were collected at room temperature at the scan speed of 5.29 deg min^{-1} by using the ω–2θ scan technique, with a scan width calculated according to the expression $0.80 \pm 0.35 \tan\theta$. Stationary background measurements were taken for a time equal to half the scan time on each side of the peak. Three standard reflections periodically measured to check the stability of the crystal showed no systematic trends. After corrections for background the intensities were calculated as described elsewhere.[31] The standard deviations $\sigma(I)$ were calculated by using the value of 0.03 for the instability factor k.[32] The intensities were corrected for the Lorentz–polarization effect, and no absorption correction was applied owing to the almost equidimensional shape of the crystal and the small absorption coefficient. Of 1896 measured reflections, 1574 were considered observed with $I \geq 3\sigma(I)$.

Structure Solution and Refinement. All calculations were carried out by using the programs SHELX76,[33] ORTEP,[34] and PLUTO[35] on a COMPAQ 386/25 PC. Atomic scattering factors for non-hydrogen atoms were taken from ref 36, while those for hydrogen atoms were taken from ref 37. Anomalous dispersion terms, both real and imaginary, were included for the non-hydrogen atoms.[38]

The function $\sum w(|F_o| - |F_c|)^2$ was minimized during the least-squares refinement, with $w = 1/\sigma^2(F_o)$. Owing to the isomorphism of $[Co_6(\mu_3\text{-}S)_8(PEt_3)_6](PF_6)$ with the analogous iron cluster,[30] the parameters of the latter were used as starting parameters. The hexafluorophosphate anion, lying on a 3-fold axis, showed disordered fluorine atom positions. Such disorder was satisfactorily resolved by postulating two different arrangements of the fluorine atoms around the same phosphorus atom (model α and $1 - \alpha$). Full-matrix least-squares refinements were carried out with anisotropic thermal parameters assigned to all atoms, except the fluorine and the hydrogens. Hydrogen atoms were introduced in their calculated positions and not refined. The refinement converged to R and R_w factors both of 0.029. Calculated coordinates of hydrogens (Table S1), thermal parameters (Table S2), and final positional parameters for non-hydrogen atoms (Table S3) are reported as supplementary material.

UV–Electronic Absorption Spectra. The CH_2Cl_2 solution electronic spectra of the complex $[Co_6(\mu_3\text{-}S)_8(PEt_3)_6](PF_6)$ were recorded at room temperature on a Shimadzu UV–visible recording spectrophotometer UV-2100.

Magnetic Measurements. The temperature dependence of the magnetic susceptibility was measured with an automated Faraday-type magnetometer equipped with an Oxford Instrument continuous flow cryostat working in the temperature range 4.2–300 K. The weight of the sample used was 8.99 mg. The diamagnetic correction applied was -882×10^{-6} emu.

EPR Spectra. Single crystals of $[Co_6(\mu_3\text{-}S)_8(PEt_3)_6](PF_6)$ were oriented using a Philips PW 1100 automated diffractometer. They are rhombohedra with well-developed principal (100), (010), (001) and centrosymmetric faces. Since the axes of the rhombohedral cell are equal, the principal faces are equivalent. The single-crystal EPR spectra were measured at variable temperature between 300 and 4.2 K using a Varian E-9 spectrometer equipped with an Oxford Instrument continuous flow cryostat by rotating the crystal along three orthogonal axes X, Y, and Z. The Z axis was chosen to be perpendicular to one of the principal faces and Y was chosen to be the intersection of two principal faces. In this way Z is parallel to one of the reciprocal axes, while Y is parallel to one of the axes of the direct cell. In agreement with the morphology of the crystal and according to a right handed choice of the reference frames, the Z and Y axes are directed along the negative sense of one reciprocal and the direct axis, respectively. Since the angle between the crystallographic axes is $\alpha = \beta = \gamma = 92.15°$, very close to 90°, the axes of the reciprocal cell are close to the axes of the direct cell, the actual angles being 3°. The X, Y, and Z axes are, therefore, parallel, within experimental error, to the direct axes and the spectra measured in the three rotations should be indistinguishable.

In order to independently check the values and directions of the $\mathbf{g}^2$ tensor, measured according to the procedure described in the next section, we mounted the crystal on a perpex rod mechanically cut at 55° from the rotation axis. In this way it is possible to align the static magnetic field along the crystallographic C_3 axis (actual angle with the perpendicular to a principal face 53.3°) and perpendicular to it.

Table II. Parameters Used in the Xα-SW Calculations for $[Co_6(\mu_3\text{-}S)_8(PH_3)_6]^+$

	I_{max}	α	sphere radius, Å
out	3	0.72610	5.432
Co	2	0.71018	1.190
P	1	0.72620	1.283
S	1	0.7247	1.279
H	0	0.7772	0.529

Calculations

Xα-SW Calculations. Xα-SW calculations have been performed on a model molecule $[Co_6(\mu_3\text{-}S)_8(PH_3)_6]^n$ (n = 0, 1±, 2±), in which the triethylphosphine ligands are replaced by phosphines. In order to avoid the use of complex basis functions, required by the actual S_6 symmetry of the cluster, we used a higher symmetry, D_{3d}, for the molecule. In this latter symmetry all the Co–S and Co–P bonds are equivalent. Relevant interatomic distances for the model compound $[Co_6(\mu_3\text{-}S)_8(PH_3)_6]^+$ are the following: Co–Co = 2.789 Å, Co–S = 2.230 Å, Co–P = 2.161 Å, P–H = 1.600 Å. The actual coordinates used in the calculations are reported in Table S4 as supplementary material.

The Xα-SW calculations were performed using the standard version of the method given in ref 39. The program used is the COOK5/TAMU1 program written by M. Cook, B. Bursten, and G. Stanley. The molecular properties were calculated according to the procedure described by Case and Karplus.[40–42] The parameters used in the calculations are listed in Table II. The α values for Co, S, and P are those tabulated by Schwarz for the free atoms,[43] while in the hydrogen sphere the spin-polarized value suggested by Slater was used.[44] The α value for the inter- and outersphere regions was determined by averaging the values used in the atomic spheres, weighted by the number of atomic valence electrons. Core levels are assumed to be confined in the atomic spheres and included in the self-consistent procedure.[35]

Spin-restricted calculations were performed for all the values of n, and spin-unrestricted calculations have been performed for n = 1±, and 2±.

The sphere radii were computed using the Norman procedure[45] and reduced by a constant factor, 0.88, to avoid excessive overlap between the atomic spheres. As is usually found for hydrogen, the Norman criterion assigns a radius which was considered to be too large on the basis of computed one-electron properties[41,42] and we used for these atoms a radius of 0.5292 Å. A tangent Watson sphere,[46] with charge opposite to that of the molecule, was placed around the charged cluster to mimic the counterion environment.

In order to compare the relative stability of the clusters with different charges, we compared the total energies and the Hellmann–Feynmann forces[47] computed on the cobalt atoms. The Hellmann–Feynman theorem is strictly obeyed by the Xα theory,[48] and the force on nucleus i exerted by the surrounding nuclei and by the electrons is given by

$$\mathbf{F}_i = -Z_i\left[\sum_{j\neq i}(Z_j\mathbf{R}_{ij}R_{ij}^{-3}) - \int(\mathbf{R}_i - \mathbf{r})|\mathbf{R}_i - \mathbf{r}|^{-3}\rho(\mathbf{r})\,d\upsilon\right] \quad (1)$$

where $\mathbf{R}_i$ represents the position of nucleus i, $\mathbf{R}_{ij} = \mathbf{R}_i - \mathbf{R}_j$, and $\rho(\mathbf{r})$ is the electronic density at point $\mathbf{r}$. When the approximations of the scattered wave procedure are introduced, and when we use different α for different atomic species, the Hellmann–Feynman theorem is only approximately followed and a non-zero force can be computed even for a molecule in its stable configuration.[49] This force depends on the dis-

(31) Bianchi, A.; Dapporto, P.; Fallani, G.; Ghilardi, C. A.; Sacconi, L. *J. Chem. Soc., Dalton Trans.* **1973**, 641.
(32) Corfield, P.; Doedens, R. J.; Ibers, J. A. *Inorg. Chem.* **1967**, *6*, 197.
(33) Sheldrick, G. M. *System of Computing Programs*; University of Cambridge: Cambridge, UK, 1976.
(34) Johnson, C. K. Rep. ORNL-5138, Oak Ridge National Laboratory, Oak Ridge, TN, 1976.
(35) Motherwell, S. *Plotting Program for Molecular Crystal Packing Diagrams*; University of Cambridge: Cambridge, UK, 1978.
(36) *International Tables for X-ray Crystallography*; Kynoch Press: Birmingham, UK, 1974; Vol. IV, p 99.
(37) Stewart, R. F.; Davidson, E. R.; Simpson, W. T. *J. Chem. Phys.* **1965**, *42*, 3175.
(38) Reference 36, p 149.
(39) Johnson, K. H. *Adv. Quantum Chem.* **1973**, *7*, 143.
(40) Case, D. A.; Karplus, M. *Chem. Phys. Lett.* **1976**, *39*, 33.
(41) Cook, M.; Karplus, M. *J. Chem. Phys.* **1980**, *72*, 7.
(42) Case, D. A.; Cook, M.; Karplus, M. *J. Chem. Phys.* **1980**, *73*, 3294.
(43) Schwartz, K. *Phys. Rev. B* **1972**, *5*, 2466.
(44) Slater, J. C. *Int. J. Quantum Chem.* **1973**, *57*, 533.
(45) Norman, J. G., Jr. *Mol. Phys.* **1976**, *31*, 1191.
(46) Watson, R. E. *Phys. Rev.* **1958**, *111*, 1108.
(47) *The Force Concept* in *Chemistry*; Deb, B. M., Ed.; Van Nostrand Reinhold: New York, 1981.
(48) Slater, J. C. *Quantum Theory of Molecules and Solids*; McGraw Hill: New York, 1974; Vol. 4.

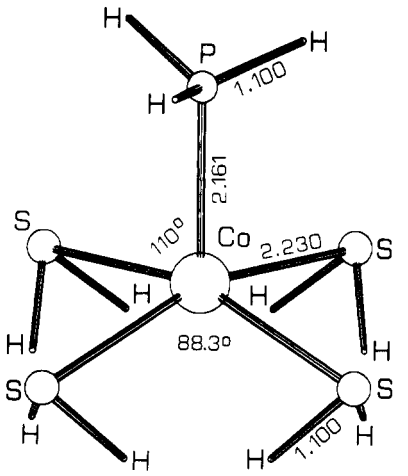

Figure 1. Geometrical features of the model complex $[Co(SH_2)_4(PH_3)]^{2+}$ used in the extended Hückel calculation. Bond distances are in Å and angles in deg.

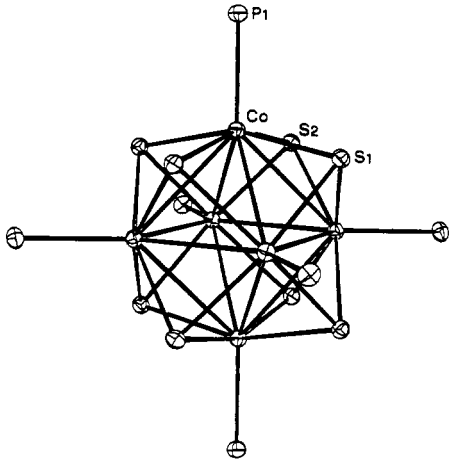

Figure 2. Perspective view of the cluster unit $[Co_6(\mu_3\text{-}S)_8(PEt_3)_6]^+$. ORTEP diagram with 30% probability ellipsoids. Only inequivalent atoms are labeled, with the C_3 axis passing through S1.

tribution of the electronic density on the molecule, and it is therefore dependent on the number of electrons and ligand type. Relative variations of the Hellmann–Feynman force recently have been used with success to rationalize the structural features of icosahedral cobalt–sulfur clusters.[18] Relative changes in the force upon adding or removing electrons are expected to reflect a change in the structure of the molecule and can thus be used as an estimate of the relative stability of the oxidation state of a molecule in a given geometrical arrangement of the atoms.

The one-electron energies and distribution of charges computed for $[Co_6(\mu_3\text{-}S)_8(PH_3)_6]^+$ are shown in Table III.

Extended Hückel calculations have been performed on a model complex $[Co(SH_2)_4PH_3)]^{2+}$ using the geometrical features shown in Figure 1 and the parameters reported in Table IV with the computer programs described in ref 50 and 51.

Extended Hückel calculations also have been performed with the parameters given in Table IV for the model complex $[Co_6(\mu_3\text{-}S)_8(PH_3)_6]^+$ used for the Xα-SW calculations, allowing small variation of the geometrical parameters in order to analyze their influence on the relative energy of the electronic levels. All the calculations have been performed on an IBM 9370/50 and on an IBM Personal System/2 Model 80/111 computer.

Results

Description of the Structure. The molecular structure of $[Co_6(\mu_3\text{-}S)_8(PEt_3)_6](PF_6)$ consists of discrete $[Co_6(\mu_3\text{-}S)_8(PEt_3)_6]^+$ cluster cations and hexafluorophosphate anions. A perspective

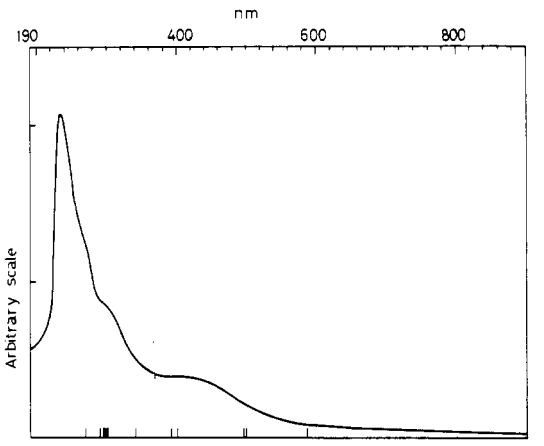

Figure 3. Graphical comparison between the computed electronic transitions and the experimental electronic spectrum of $[Co_6(\mu_3\text{-}S)_8(PEt_3)_6](PF_6)$.

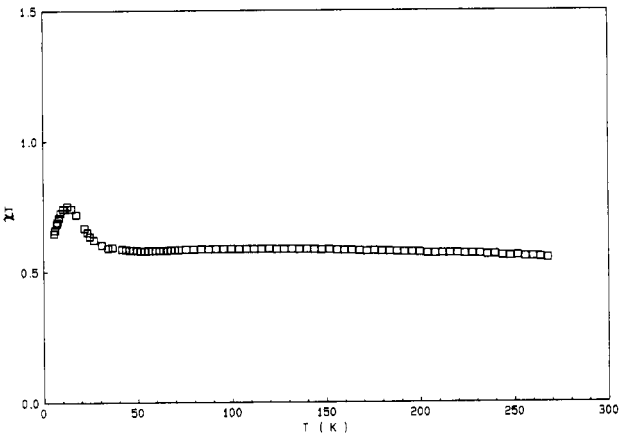

Figure 4. Observed temperature dependence of the magnetic susceptibility for $[Co_6(\mu_3\text{-}S)_8(PEt_3)_6](PF_6)$ in the range 291–6 K in the form χT vs T.

view of the cation is given in Figure 2; selected bond distances and angles are reported in Table V.

The cation, which is isostructural with all the members of the series $[M_6S_8(PEt_3)_6]^{n+}$ (M = Fe, n = 1,[30] 2;[52] Co, n = 0, 1[28]), is built up of an octahedral cluster of cobalt atoms with all the faces symmetrically capped by triply bridging sulfur ligands. Each metal atom is additionally linked to a triethylphosphine fragment. The crystallographic symmetry is $C_3 \otimes i$, but the symmetry of the inner core is very close to O_h. Bond distances and angles match very well the values already reported for the corresponding cluster $[Co_6(\mu_3\text{-}S)_8(PEt_3)_6]^+$, obtained as tetraphenylborate salt.[28]

UV–ELectronic Absorption Spectra. The solution electronic spectrum of $[Co_6(\mu_3\text{-}S)_8(PEt_3)_6](PF_6)$ is shown in Figure 3, where the computed transitions are also indicated. Details on the calculation and the assignment will be given in the next sections.

Magnetic Measurements. The measured temperature dependence of the magnetic susceptibility of $[Co_6(\mu_3\text{-}S)_8(PEt_3)_6](PF_6)$ in the range 291–6 K is shown in Figure 4 in the form χT vs T. The observed effective magnetic moment, μ_{eff}, is 2.31 μ_B at 290 K, it reaches a maximum value of 2.71 μ_B at 13 K, and it decreases below this temperature. The value measured at 4.2 K is 2.46 μ_B.

EPR Spectra. $[Co_6(\mu_3\text{-}S)_8(PEt_3)_6](PF_6)$ is EPR silent from room temperature to ≈20 K. Below this temperature a signal grows up and sharpens on decreasing the temperature. A similar behavior has been previously observed[29] for $[Co_6(\mu_3\text{-}S)_8(PEt_3)_6](BPh_4)$. The cluster is EPR silent at room temperature even in dilute solutions. The single-crystal EPR spectra, recorded at 4.2 K, showed a single resonance in all the crystal orientations,

(49) *Local Density Approximations in Quantum Chemistry and Solid State* Physics; Dahl, J. P., Avery, J., Eds.; Plenum Press: New York, 1984.
(50) Hoffmann, R.; Fujimoto, J. R.; Swenson, C.; Wan, C. C. *J. Am. Chem. Soc.* **1973**, *95*, 7644.
(51) Mealli, C.; Proserpio, D. M. *J. Chem. Educ.* **1990**, *67*, 399.
(52) Cecconi, F.; Ghilardi, C. A.; Midollini, S. *J. Chem. Soc., Chem. Commun.* **1981**, 640.

Table III. One-Electron Energies and Distribution of Charges for $[Co_6(\mu_3\text{-}S)_8(PH_3)_6]^+$

level	energy, eV	Co	P	S_I	S	H_I	H	Int	Out
$11A_{2g}$	-3.975	52	0	9	27	0	0	12	0
$14E_g$	-4.584	50	0	6	29	0	0	15	0
$11A_{1g}$	-4.584	50	0	14	21	0	0	15	0
$14E_u$	-4.726	45	0	11	31	0	0	13	0
$13E_g$	-4.972	56	15	4	12	1	1	11	0
$10A_{2g}$	-5.232	53	16	0	18	0	1	11	1
$13E_u$	-5.256	53	16	6	11	1	1	11	1
$12E_u$	-7.059	61	1	2	22	0	1	12	0
$9A_{2u}$	-7.060	61	1	14	11	1	0	12	0
$11E_u$	-7.196	81	0	5	9	0	0	5	0
$4A_{1u}$	-7.196	81	0	0	14	0	0	5	0
$10A_{1g}$	-7.201	54	21	9	1	1	1	21	0
$12E_g$	-7.341	57	0	14	23	0	0	6	0
$4A_{2g}$	-7.345	57	0	0	37	0	0	6	0
$11E_g$	-7.472	68	1	3	15	0	1	11	0
$9A_{1g}$	-7.512	69	1	8	8	1	1	12	0
$3A_{2g}$	-7.663	96	0	0	0	0	0	3	0
$2A_{2g}$	-7.776	41	2	0	39	0	3	15	0
$10E_g$	-7.778	41	2	15	25	1	2	15	0
$9E_g$	-7.842	89	1	1	3	0	0	6	0
$3A_{1u}$	-7.845	83	2	0	4	0	3	9	0
$10E_u$	-7.861	83	2	1	2	1	1	9	0
$9E_u$	-9.134	40	1	14	31	0	0	14	0
$8A_{2u}$	-9.138	40	1	6	38	0	0	14	0
$2A_{1u}$	-9.989	27	13	0	35	0	6	18	0
$8E_u$	-10.024	36	9	23	13	2	2	15	0
$7E_u$	-10.087	45	3	0	39	1	1	11	0
$8A_{1g}$	-10.098	26	10	31	12	3	2	16	0
$8E_g$	-10.157	29	13	0	36	1	5	16	0
$7E_g$	-10.180	34	3	15	33	0	1	13	0
$7A_{2u}$	-10.203	41	1	16	33	0	0	9	0
$7A_{1g}$	-10.234	35	6	0	42	2	1	14	0
$6E_g$	-10.369	40	43	0	2	1	3	9	0
$6A_{2u}$	-10.398	34	35	7	6	5	0	12	1
$6E_u$	-10.410	35	38	0	10	0	5	11	1
$5E_u$	-10.537	8	39	1	14	4	10	24	1
$5A_{2u}$	-10.544	10	41	5	8	4	9	23	1
$6A_{1g}$	-10.675	37	34	3	10	1	2	12	0
$5E_g$	-11.024	4	43	1	2	9	10	32	0
$1A_{2g}$	-11.026	4	44	0	2	0	18	32	0
$5A_{1g}$	-11.184	19	30	5	9	8	4	25	0
$4E_u$	-11.199	7	33	6	10	7	6	30	0
$4E_g$	-11.213	18	30	4	10	2	9	26	0
$1A_{1u}$	-11.216	7	32	0	17	0	12	30	1
$4A_{1g}$	-11.325	21	6	13	37	0	0	22	0
$3E_u$	-11.449	21	17	4	30	0	5	22	0
$4A_{2u}$	-11.453	21	17	19	14	5	1	22	0
$3E_g$	-11.662	26	6	11	35	0	1	20	0
$3A_{1g}$	-17.977	4	73	1	2	2	4	14	0
$3A_{2u}$	-17.978	4	73	2	1	2	4	13	1
$2E_u$	-17.979	4	73	0	3	2	4	13	1
$2E_g$	-18.061	4	74	0	0	2	4	14	1
$2A_{2u}$	-18.850	9	0	22	63	0	0	6	0
$2A_{1g}$	-18.997	7	0	64	21	0	0	8	0
$1E_g$	-19.013	7	0	0	85	0	0	8	0
$1A_{2u}$	-19.607	8	2	58	21	0	0	10	0
$1E_u$	-19.621	8	2	0	79	0	0	10	0
$1A_{1g}$	-20.437	11	2	18	57	0	0	11	0
Co(3p)	-63.784	100	0	0	0	0	0	0	0
Co(3s)	-97.967	100	0	0	0	0	0	0	0
P(2p)	126.878	0	100	0	0	0	0	0	0
S(2p)	-157.703	0	0	100	0	0	0	0	0
S(2p)	-157.798	0	0	0	100	0	0	0	0
P(2s)	-174.666	0	100	0	0	0	0	0	0
S(2s)	-210.784	0	0	100	0	0	0	0	0
S(2s)	-210.877	0	0	0	100	0	0	0	0
Co(2p)	-765.874	100	0	0	0	0	0	0	0
Co(2s)	-880.646	100	0	0	0	0	0	0	0
P(1s)	-2078.151	0	100	0	0	0	0	0	0
S(1s)	-2396.665	0	0	100	0	0	0	0	0
S(1s)	-2396.777	0	0	0	100	0	0	0	0
Co(1s)	-7509.503	100	0	0	0	0	0	0	0

in agreement with the presence of one magnetically non-equivalent cluster in the unit cell.[53] The observed angular dependence of

Table IV. Valence Ionization Potentials and Coefficients and Exponents of the Atomic Slater Functions Used in the Extended Hückel Calculations

atom	orbital type	IP, eV	c_1	ζ_1	c_2	ζ_2
Co	3d	-13.18	0.57465	5.55	0.6131	2.00
	4s	-9.21	1.00000	2.00		
	4p	-5.29	1.00000	2.00		
P	3s	-18.60	1.00000	1.60		
	3p	-14.00	1.00000	1.60		
H	1s	-13.60	1.00000	1.30		

Table V. Selected Bond Distances (Å) and Angles (deg)

Distances			
Co–Co[a]	2.788 (1)	Co–S2[c]	2.232 (1)
Co–Co[b]	2.788 (1)	Co–S2[a]	2.218 (1)
Co–S1	2.236 (1)	Co–P1	2.161 (1)
Co–S2	2.223 (1)		
Angles			
Co[a]–Co–Co[b]	90.0	P1–Co–S1	102.4 (1)
Co[a]–Co–Co[d]	60.0	P1–Co–S2	103.3 (1)
Co[b]–Co–Co[d]	60.0 (1)	P1–Co–S2[a]	98.7 (1)
S1–Co–S2	87.6 (1)	P1–Co–S2[c]	99.7 (1)
S1–Co–S2[a]	87.8 (1)	Co–S1–Co[a]	77.1 (1)
S1–Co–S2[c]	157.9 (1)	Co–S2–Co[b]	77.5 (1)
S2–Co–S2[a]	158.1 (1)	Co–S2–Co[d]	77.8 (1)
S2–Co–S2[c]	88.1 (1)	Co[b]–S2–Co[d]	77.6 (1)
S2[a]–Co–S2[c]	88.2 (1)		

[a] z,x,y. [b] −z,−x,−y. [c] −y,−z,−x. [d] y,z,x.

Table VI. Principal Values and Directions[a] of the g^2 Tensor for $[Co_6(\mu_3\text{-}S)_8(PEt_3)_6](PF_6)$

g_1	2.02 (2)	0.4 (4)	0.80 (4)	−0.4 (4)
g_2	2.04 (1)	−0.7 (3)	0.5 (4)	−0.7 (3)
g_3	2.24 (2)	−0.57 (3)	0.60 (3)	−0.56 (3)

[a] The directions are given as direction cosines in the X, Y, Z reference frame (see text).

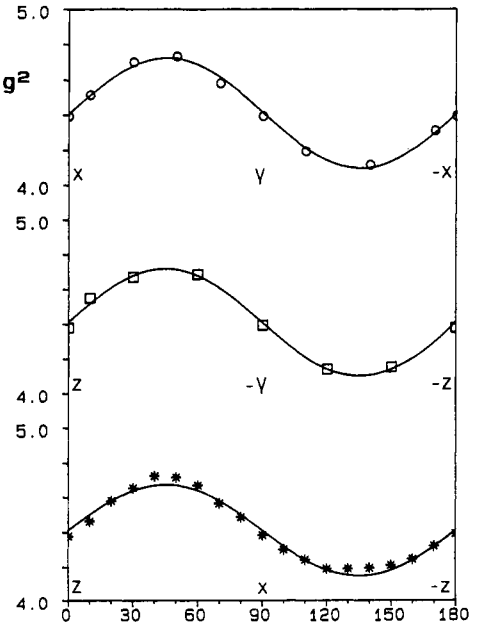

Figure 5. Observed and calculated (solid lines) angular dependence of the g^2 values in the planes orthogonal to Y (*), X (□), and Z (○) for $[Co_6(\mu_3\text{-}S)_8(PEt_3)_6](PF_6)$.

the g^2 tensor in the XZ, YZ, and XY planes is shown in Figure 5. The data have been fitted using a $S = {}^1/_2$ spin hamiltonian with a least-squares fitting procedure based on the Schönland method.[54] The principal values and directions of g^2 are shown

(53) Bencini, A.; Gatteschi, D. *Transition Metal Chemistry*; Melson, G. A., Figgis, B. N., Eds.; Marcel Dekker: New York, 1982; Vol. 8, p 1.
(54) Schönland, R. S. *Proc. Phys. Soc.* **1959**, *73*, 78.

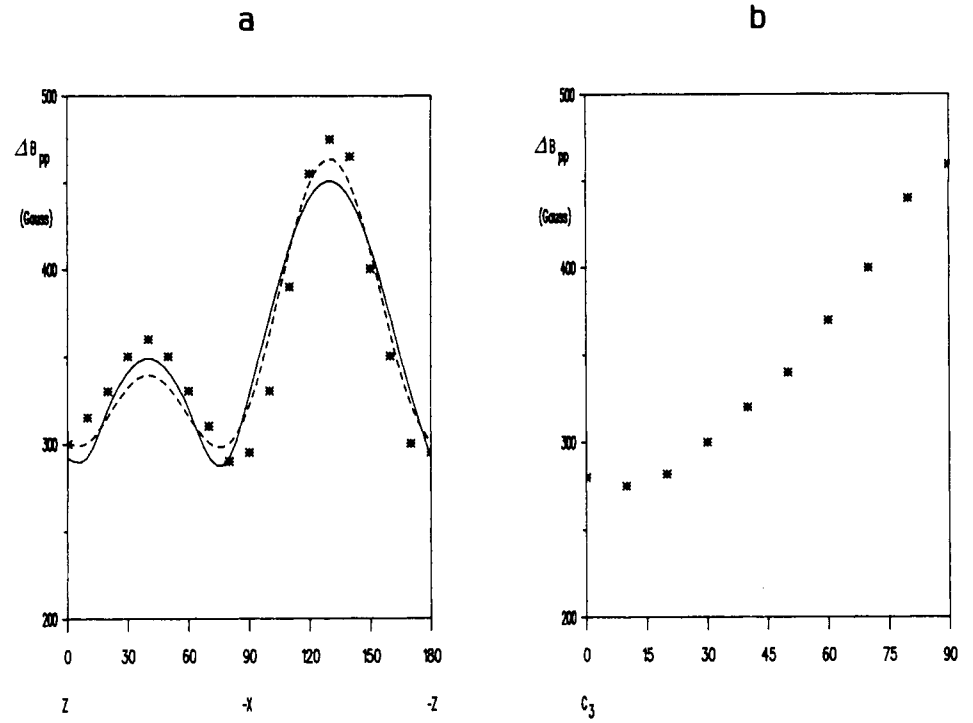

Figure 6. Observed angular dependence of the ΔB_{pp} of the EPR signal in the XZ plane (a) and in a plane containing the C_3 axis (b) for $[Co_6(\mu_3\text{-}S)_8(PEt_3)_6](PF_6)$. The best fit curves obtained using the equation $\Delta B_{pp} = \alpha + \beta(3\cos^2\theta - 1)^\gamma$ with $\gamma = {}^4/_3$ (solid line) and $\gamma = 2$ (dashed line) are also shown in the XZ plane.

in Table VI. The measured tensor is axial in agreement with the crystallographic site symmetry of the cluster, S_6, therefore the direction cosines of g_1 and g_2 are affected by the symmetry indetermination. The g_3 value shown in Table VI is 3° with the crystallographic C_3 axis when X, Y, and Z are chosen according to the crystal morphology. The g values measured parallel and perpendicular to the C_3 axis are $g_\parallel = 2.26$ and $g_\perp = 2.07$, well in agreement with the values measured with the Schönland procedure.

The observed angular dependence of the peak-to-peak line width of the signal, ΔB_{pp}, is reported in Figure 6a. Since the three planes are identical within experimental error, only the angular dependence of the signal observed in the XZ plane is shown. In each plane the line width has two maxima, 360 and 480 G, respectively, 90° apart and a minimum roughly at 50° from the absolute maximum. The observed angular dependence of ΔB_{pp} in a plane containing the C_3 axis is reported in Figure 6b. In Figure 6a the solid lines represent the best fit curves obtained using the equation

$$\Delta B_{pp} = \alpha + \beta(3\cos^2\theta - 1)^\gamma \qquad (2)$$

with $\alpha = 282$, $\beta = 67$, $\gamma = 4/3$ (solid line) and $\alpha = 280$, $\beta = 42$, $\gamma = 2$ (dashed line). The fitting procedure was based on a Simplex minimization routine which minimized the function

$$F = \sum(\Delta B_{pp}^{\circ} - \Delta B_{pp}^{c})^2 \qquad (3)$$

where ΔB_{pp}° and ΔB_{pp}^{c} are the observed and computed peak-to-peak line widths, respectively, and the summation runs over the experimental points.

Discussion

We will discuss shortly the crystal and molecular structure of $[Co_6(\mu_3\text{-}S)_8(PEt_3)_6]^+$, and in the first part of this section we will give a rather phenomenological interpretation of the EPR spectra and of the magnetic behavior. In the last part of this section we will discuss the results of the Xα-SW calculations performed on the model molecule $[Co_6(\mu_3\text{-}S)_8(PH_3)_6]$, and we will present a molecular orbital interpretation of the electronic structure of the clusters based on the results obtained for this model complex.

Crystal Structure. The $[Co_6(\mu_3\text{-}S)_8(PEt_3)_6]^+$ cation in the hexafluorophosphate salt has a crystallographic S_6 symmetry, the highest actually seen in the $[M_6S_8(PEt_3)_6]^{n+}$ (with M = Co, n = 0, 1; M = Fe, n = 1, 2) series of complexes.[28,30,52] The crystallographic C_3 axis passes through two centrosymmetric sulfur atoms, S_1 and $S_{1'}$. The coordination geometry around the cobalt centers is close to a square pyramid with the phosphorus atom of the triethylphosphine ligand in the axial position. The Co–S bond distances are in the range 2.22–2.24 Å (av 2.23 Å), the longest value corresponding to Co–S_1. The in-plane S–Co–S angles are 88°, the S–Co–P angles range from 99° to 103° (av 101°), and the Co–P bond length is 2.16 Å. The above geometry compares well with that seen in the tetraphenylborate salt. In the latter complex the six cobalt atoms are, however, not related by symmetry operations. The geometrical parameters around the cobalt atoms are, anyway, equal within experimental error, and the low symmetry of the complex is probably due to the BPh_4^- anion which prevents the occurrence of a C_3 axis.

Nature of the Ground State. The single-crystal EPR spectra of $[Co_6(\mu_3\text{-}S)_8(PEt_3)_6](BPh_4)$, recorded at 4.2 K, have been previously reported.[29] They were interpreted using a $S = {}^1/_2$ spin hamiltonian with $g_x = 2.35$ (1), $g_y = 2.04$ (1), and $g_z = 1.95$ (1). The z axis was found at 16° from one of the six inequivalent cobalt–phosphorus bonds, namely Co_4–P_4, and x is 17° from a cobalt–sulfur bond. Since the overall structure is not far from being centrosymmetric, the x, y, and z magnetic axes are also parallel to the quasisymmetric bonds around Co_2. A schematic view of the magnetic axes with respect to the cluster cation is shown in Figure 7. The g values compare well with those observed in other square-pyramidal low-spin cobalt(II) complexes,[53] and this suggests a localization of the unpaired electron on one of the six cobalt centers, either Co_2 or Co_4.

The correlation of the g values to the electronic and geometrical structure of low-spin cobalt(II) complexes is not completely straightforward. As already pointed out by Daul, Schläpfer, and von Zelewsky,[55] the ground state of these complexes is an admixture of doublets and quartet states. In a ligand field framework, even neglecting the low-lying quartet states, a low-spin d^7 configuration cannot be properly described by one isolated doublet state, like a d^9 system, but several doublet states, having the unpaired electron in the xy, xz, yz, and z^2 orbitals, respectively,

(55) Dual, c.; Schlaepfer, C. W.; von Zelewsky, A. *Struct. Bonding (Berlin)* **1979**, *36*, 129.

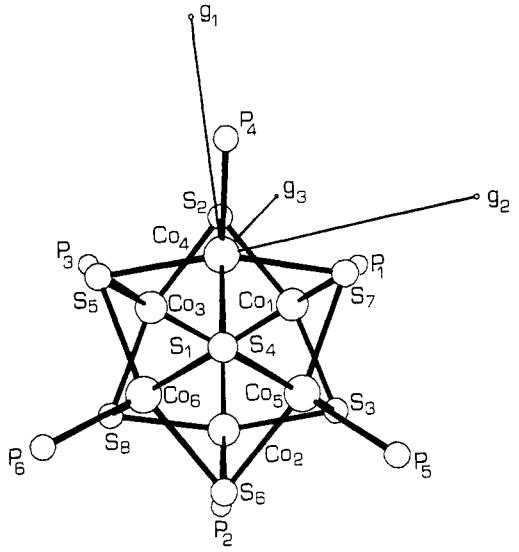

Figure 7. Orientation of the **g** tensor in the molecular frame looking down the pseudo-C_3 axis for $[Co_6(\mu_3\text{-}S)_8(PEt_3)_6](BPh_4)$.

are quite close in energy and spin–orbit coupling is therefore important in determining the nature of the ground state.[53] Of course low-symmetry components of the ligand field can also cause mixing of the d orbitals, but these have been generally neglected for the sake of simplicity. The interelectronic interaction places the doublet state with the unpaired electron in the xy orbital 20B (B is the Racah parameter, $\cong$1115 cm^{-1}) higher in energy than that with the unpaired electron in the z^2 orbital, and 15B higher than those with the unpaired electron in the xz and yz orbitals. Neglecting the contribution of the doublet state with the unpaired electron in the xy orbital in the analysis of the EPR spectra, one is led to a three-parameter model in which the ground Kramers doublet has the form[56]

$$|\psi\pm\rangle = a|yz\mp\rangle + b|z^2\pm\rangle + c|xz\mp\rangle \qquad (4)$$

where $|d\pm\rangle$ represents the configuration with the unpaired electron with spin α or β, respectively, in the orbital d. The g values can thus be expressed as

$$\begin{aligned} g_x &= g_e(a^2 + b^2 - c^2) - 4\sqrt{3}ab \\ g_y &= g_e(-a^2 + b^2 + c^2) - 4\sqrt{3}bc \\ g_z &= g_e(-a^2 + b^2 - c^2) + 4\sqrt{3}ac \end{aligned} \qquad (5)$$

with the normalization condition $a^2 + b^2 + c^2 = 1$. A reasonable fit of the g values of $[Co_6(\mu_3\text{-}S)_8(PEt_3)_6](BPh_4)$ using a, b, and c as free parameters is obtained with $a = -0.051$, $b = 0.998$, $c = -0.0071$, which yields $g_x = 2.35$, $g_y = 2.04$, and $g_z = 1.99$. It is apparent that all the anisotropy of the **g** tensor is related to a different mixing of the xz and yz orbitals in the ground state. This effect was found to be large in low-spin cobalt(II) bis chelate complexes and was ascribed to anisotropic π interactions characteristic of the chelating nature of the ligand.[56-58] In the present complex these interactions are absent and surely the above values are strongly influenced by the approximations used in deriving eq 4, in particular neglect of quartet state admixture and low-symmetry components of the ligand field. In order to have more insight into the electronic structure of the complex, we can look to the results of the extended Hückel calculations we have performed on the model complex $[Co(SH_2)_4(PH_3)]^{2+}$. The SH_2 groups have been used instead of S^{2-} anions in order to mimic the μ_3 bonding mode of the sulfur atoms in the cluster complex. The LCAO composition of the LUMO's and HOMO's, mainly d metal in character, is schematically shown in Figure 8. The LUMO is MO = 16. It is mainly x^2-y^2, it is highly destabilized by the σ interaction with the sulfurs, and its energy is $3e_\sigma^S$ within the angular overlap model of the ligand field.[59,60] The unpaired electron is contained in one of the four lower lying orbitals, the three remaining ones being double occupied. The different occupancy gives rise to the different doublet states, whose relative energy cannot, however, be computed with the extended Hückel method, which does not include electron exchange effects. The z^2 orbital, MO = 17, has σ interactions with both the sulfur and the phosphorus atoms, $e_\sigma^S + e_\sigma^P$ in the AOM, and it lies $\approx$1.4 eV below the x^2-y^2 orbital. The xz and yz orbitals give π interactions with sulfurs and lie $\approx$2 eV below; the xy orbital is nonbonding. It is apparent from Figure 7 that the xz and yz orbitals will be degenerate unless some difference in the bond lengths and/or angles exists between the sulfur atoms on the x and y axes. In this simple picture the **g** anisotropy is thus related to differences in bond lengths and angles between the equatorial sulfurs, and therefore to the low symmetry of the local environment around the cobalt atoms in the cluster.

It is not a matter now to proceed further in the discussion of the EPR spectra of $[Co_6(\mu_3\text{-}S)_8(PEt_3)_6](BPh_4)$, since it is apparent that the number of parameters required in any more sophisticated model largely exceeds the number of available experimental data. The above discussion has shown that the observed EPR spectra can be consistent with an unpaired electron localized on one cobalt center in the cluster.

The EPR spectra of $[Co_6(\mu_3\text{-}S)_8(PEt_3)_6](PF_6)$ are axial and conform to the crystallographic site symmetry. The calculation of the **g** tensor in polynuclear complexes is not a straightforward procedure.[10] The bonding interactions between the paramagnetic centers are generally mediated by ligands, and this results in the so-called weak bonding interaction, which, for example, is responsible of the appearance of multiplets of states with different total spin thermally populated in a wide temperature range. This structure cannot generally be properly accounted for by molecular orbital methods based on a single Slater determinant, and extensive use of configuration interaction is needed.[11] Also methods based on the use of broken symmetry determinants (VB-Xα) have been successfully applied in a number of cases.[11,61] The magnetic properties of polynuclear transition metal complexes can thus be generally rationalized using a Heitler–London type wave function, which, for example, allowed the Zeeman and hyperfine tensors of polynuclear complexes to be expressed as linear combinations of **g** and **A** tensors centered on the individual paramagnetic centers. In the usual approximation that the weak bonding interactions do not severely alter the relative energies of the excited states localized on each center with respect to an isolated complex with the same coordination, the magnetic parameters of the individual centers in the polynuclear complex are usually taken equal to those of the isolated moieties and used to interpret the magnetic structure of the polynuclear molecule.[10] This approximation also has been applied to mixed valence clusters.[6,14,15]

The $[Co_6(\mu_3\text{-}S)_8(PEt_3)_6](PF_6)$ falls in the class of the "mixed valence" clusters. If we assign a formal 2- charge to each sulfur atom we compute a formal charge of 3+ for five cobalt centers and 2+ for one of them. Since the metals are equivalent by symmetry we must conclude that the extra electron added to one cobalt is delocalized on the whole molecule. A convenient way to look at the electronic structure of mixed valence complexes, in the weak bonding approximation, is to write the wave function representing the ground state of the cluster as an antisymmetrized product of functions representing the ground state of each metal center[62,63]

$$|\psi_j\rangle = \prod_{i \neq j} |i\rangle|j^*\rangle \qquad (6)$$

(56) Ceulemans, A.; Debuyst, R.; Dejehet, F.; King, G. S. D.; Vanhecke, M.; Vanquickenborne, L. G. *J. Phys. Chem.* **1990**, *94*, 150.
(57) Ceulemans, A.; Dendooven, M.; Vanquickenborne, L. G. *Inorg. Chem.* **1985**, *24*, 1153.
(58) Ceulemans, A.; Dendooven, M.; Vanquickenborne, L. G. *Inorg. Chem.* **1985**, *24*, 1159.
(59) Schäffer, C. E.; Jorgensen, C. K. *Mol. Phys.* **1965**, *9*, 401.
(60) Bencini, A.; Benelli, C.; Gatteschi, D. *Coord. Chem. Rev.* **1984**, *60*, 131.
(61) Noodleman, L.; Case, D. A. *J. Chim. Phys.* **1989**, *86*, 743.

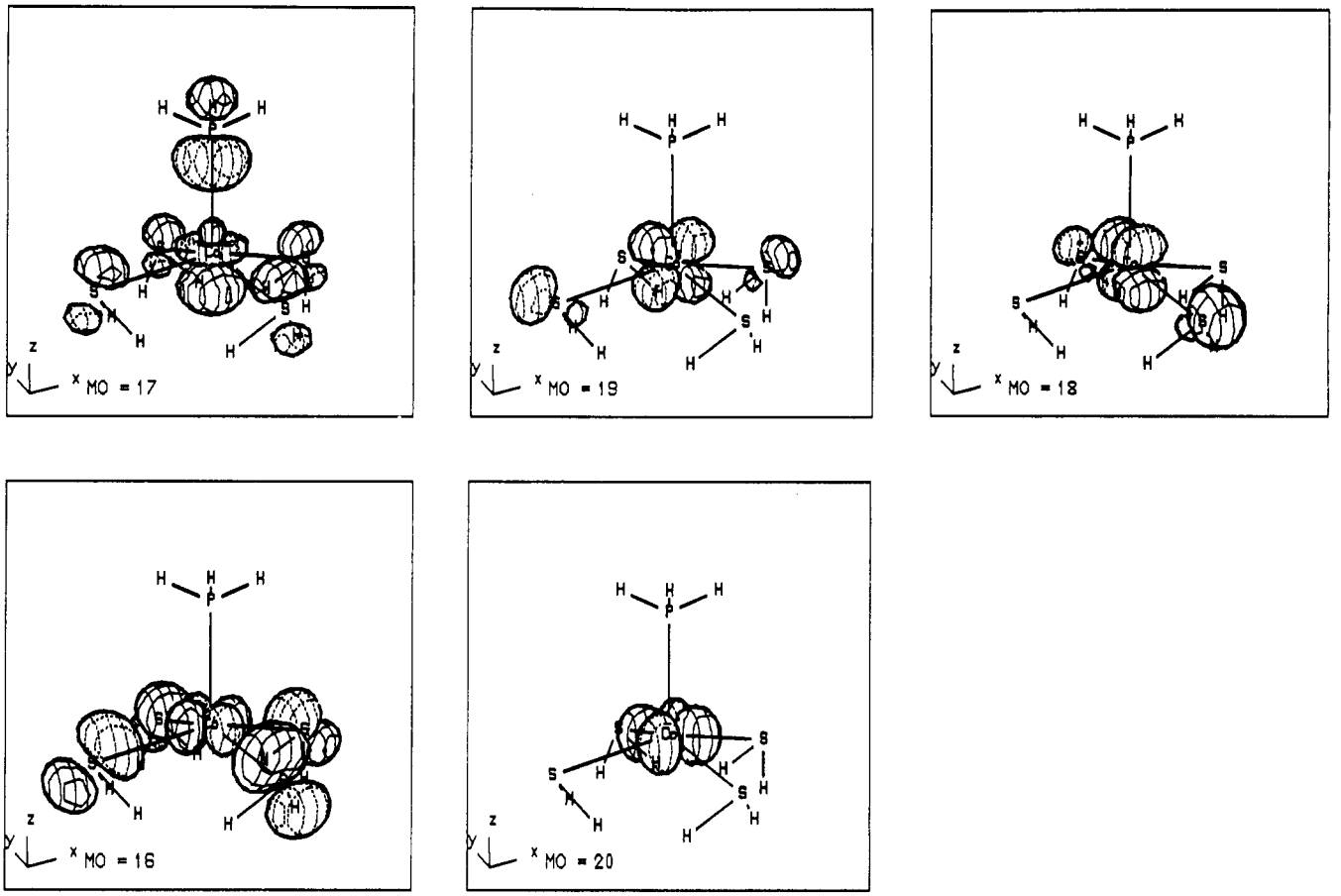

Figure 8. LCAO composition of LUMO and HOMO for $[Co(SH_2)_4PH_3]^{2+}$.

where the asterisk indicates that the extra electron is on center j. This wave function describes a state with the unpaired electron localized on center j and, since the cobalt(III) ions are diamagnetic, must have a **g** tensor equal to that observed in $[Co_6(\mu_3\text{-}S)_8(PEt_3)_6](BPh_4)$ when $|j^*\rangle$ represents the ground Kramers doublet. This will allow us to interpret the EPR spectra of the present cluster without the exact knowledge of the nature of the excited states. Six functions of the above type, corresponding to the six possibilities of localizing the electron, are equivalent descriptions of the ground state of the localized cluster and correspond to six degenerate states. When electron delocalization occurs, the above functions do not represent the proper eigenstate of the system, since they do not respect its symmetry. This causes a splitting of the six degenerate states in the so-called "resonance split multiplets."[64] The actual symmetry of the cluster, $S_6 = C_3 \otimes i$, groups the six product functions $|\psi_j\rangle$ according to the character table of the point group in A and E type functions of the form

$$|\psi_A\rangle = N\sum_j |\psi_j\rangle$$
$$|\psi_{E1}\rangle = N[|\psi_1\rangle + |\psi_5\rangle + \epsilon(|\psi_2\rangle + |\psi_6\rangle) + \epsilon^*(|\psi_3\rangle + |\psi_4\rangle)]$$
$$|\psi_{E2}\rangle = N[|\psi_1\rangle + |\psi_5\rangle + \epsilon^*(|\psi_2\rangle + |\psi_6\rangle) + \epsilon(|\psi_3\rangle + |\psi_4\rangle)] \quad (7)$$

where N are appropriate normalization constants and $\epsilon = e^{2\pi i/3}$. The hamiltonian which describes the valence electron can be written as the sum of the kinetic energy of the electron and the coulomb attraction from the nuclei

$$H = -\hbar^2/2m\nabla^2 - \sum_i Ze^2/r_i \quad (8)$$

r_i being the distance of the electron from nucleus i. Apart from constant diagonal terms, the hamiltonian matrix contains the delocalization parameters $p_{ij} = \langle\psi_i|H|\psi_j\rangle$. In principle three delocalization parameter should be taken into account, namely p, p', and p'' connecting the metal centers related by the C_3 axis, by the inversion center i and by the $C_3 \otimes i$ operations, respectively. p is expected to be larger than both p' and p'', and assuming $p' = p'' = 0$, diagonalization of the hamiltonian matrix gives resonance split multiplets with the following relative energies: $E(^2A_g) = 3p$, $E(^2E_g) = 0$, $E(^2A_u) = p$, $E(^2E_u) = -2p$. When p is negative, the ^2A_g state is the ground state of the system. Allowing for non-zero p' and p'' parameters, always assuming $p' = p''$, alters the relative spacing of the levels, but it does not change the nature of the ground state. The form of the ground state suggests that the **g** tensor of the delocalized cluster can be written as

$$\mathbf{g} = (1/6)\sum_i \mathbf{g}_i \quad (9)$$

where $\mathbf{g}_i$ is the **g** tensor expected when the extra electron is localized on center i. Using in (9) the principal values seen in $[Co_6(\mu_3\text{-}S)_8(PEt_3)_6](BPh_4)$ and placing the z_i axes parallel to the cobalt–phosphorus bonds we compute a **g** tensor which, upon diagonalization, yields $g_\parallel = 2.22$ (2) and $g_\perp = 2.06$ (2). These values compare well with the experimental values 2.24 (2) and 2.03 (2).

Magnetic Interactions. The temperature dependence of the effective magnetic moment shows a net maximum around 20 K. Although the magnetism of low-spin cobalt complexes is highly influenced by low-lying quartet states and by the relevant mixing of excited doublet states into the ground state,[55,65] an increase of the magnetic moment with a decrease in temperature requires the population of high-spin state at low temperature, contrary to the above analysis of the ground state of the mixed valence cluster. The observed χT vs T curve can be expected if a weak magnetic interaction exists between the paramagnetic clusters in the solid

(62) Tsukerblat, B. S.; Belinski, M. I.; Fainzil'berg, V. E. *Sov. Chem. Rev.* **1987**, *9*, 339.
(63) Belinski, M. I. *Mol. Phys.* **1987**, *60*, 793.
(64) Anderson, P. W. In *Magnetism*; Rado, G. T., Suhl, H., Eds.; Academic Press: New York, 1963; Vol. 1, p 25.
(65) Reuveni, A.; Malatesta, V.; McGarvey, B. R. *Can. J. Chem.* **1977**, *55*, 70.

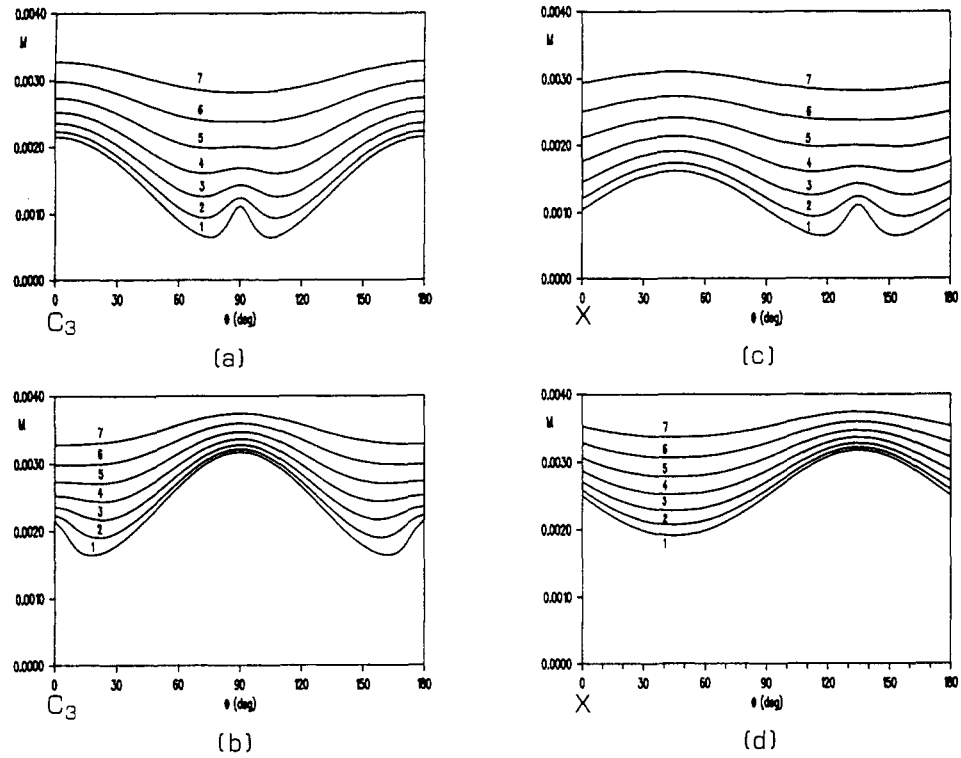

Figure 9. Angular dependence of the calculated second moment relative to the hyperfine interaction in a plane containing the C_3 axis (a and b) and in the XZ plane (c and d) with the following: (a and c) $A_\parallel > A_\perp$ with $A_\parallel/A_\perp$ = 6.67 (1), 4.00 (2), 2.86 (3), 2.22 (4), 1.82 (5), 1.54 (6), 1.33 (7); (b and d) $A_\parallel < A_\perp$ with $A_\perp/A_\parallel$ = 6.67 (1), 4.00 (2), 2.86 (3), 2.22 (4), 1.82 (5), 1.54 (6), 1.33 (7).

state, and similar behavior has already been observed in low-dimensional magnetic systems.[4,66]

In order to have more information about the nature of this interaction we have measured the angular dependence of the ΔB_{pp} of the EPR signal at 4.2 K as described in the Experimental Section. The observed angular dependence strongly resembles that measured in mono- and bi-dimensional magnetic systems when dipolar interactions are dominant over the Zeeman and exchange terms,[10] and in Figure 6a we have reported the best fit curves computed using the equation $\alpha + \beta(3\cos^2\theta - 1)^\gamma$, which was found to hold in one-dimensional systems ($\gamma = {}^4/_3$) and two-dimensional systems ($\gamma = 2$). In both cases the smallest line width is computed at 54.7° from the maximum. This maximum coincides with the chain axis or with the perpendicular to the magnetic plane for $\gamma = {}^4/_3$ and 2, respectively. A similar angular dependence of the line width of the EPR signal was observed also in the *ab* plane of the $[Co_6(\mu_3\text{-}S)_8(PEt_3)_6](BPh_4)$ salt, and the existence of a magnetic interaction between the cluster molecule in the solid state was suggested.[29]

Unresolved hyperfine splitting can be responsible for large anisotropy in the line width of EPR signals,[10,29] and its effects in the present case should be taken into consideration since we have contributions at least from six cobalt nuclei. In the rotation around a direction perpendicular to the C_3 axis (Figure 6b) we have indeed found some anisotropy in the line width which has a minimum along the C_3 axis (parallel direction).

Since we have no experimentally available data on the hyperfine coupling with the cobalt nuclei, which in low-spin cobalt(II) complexes was found to vary widely, we have performed sample calculations of the second moments of the absorption curve using the formulae previously reported for an axial hyperfine tensor[10,29] varying the ratio between $A_\parallel$ and $A_\perp$. The results of our calculations are shown in Figure 9. On the left-hand side (Figure 9, a and b) we show the angular dependence of the second moment computed with the static magnetic field moving from a direction parallel to C_3 ($\theta = 0°$) to a direction perpendicular to it. Only some of the curves computed with $A_\perp > A_\parallel$ (Figure 9b) do not show any relative minimum and are comparable with the measured angular dependence of the line width reported in Figure 6b. In Figures 9c and 9d the second moments computed with the static magnetic field in the XY laboratory plane are shown. With the above choice of the relative magnitude of $A_\parallel$ and $A_\perp$ no curve can reproduce the experimental data.

The observed angular dependence of the line width cannot therefore be completely ascribed to anisotropy of unresolved hyperfine splitting and, supporting the magnetic data, suggests that some interaction should be operative between the clusters. The EPR spectra show that, at 4.2 K, the dominant interaction is dipolar in origin and has a minimum value along the C_3 axis. A schematic view of the packing is shown in Figure S1 (supplementary material). Along the C_3 axis the magnetic clusters are intercalated by the diamagnetic PF_6^- ions, which reduces the transmission of a magnetic interaction.

MO Calculations. The interpretation of the experimental data collected on the $[Co_6(\mu_3\text{-}S)_8(PEt_3)_6]^+$ cation in two different salts gave some information on the nature of the electronic ground state of the cluster and on the existence of extended magnetic interactions in the solid state. A molecular orbital description of the magnetic observables is not possible, due to the limitations of the molecular orbital approaches, but we can use the molecular orbital theory to compare bonding features and the relative stability of the cluster in different oxidation states. The results of the Xα-SW calculations on the model molecule $[Co_6(\mu_3\text{-}S)_8(PH_3)_6]^+$ and the parameters used are described in the Experimental Section. In Table III the one-electron energy levels and charge distribution are reported. All the energy levels up to $9A_{2u}$ are fully occupied. The HOMO is the $12E_u$ level which contains 3 electrons, the total number of electrons being 397. We have found that adding up to 3 electrons or removing 1 electron causes the charge of the molecule to pass from n = 1+ to 0, 1−, 2±, but it does not significantly alter the energy level ordering and the charge distribution computed for n = 1+, except for a common shift of the absolute value of the one-electron energies due to the different charges of the Watson sphere.[67] Therefore we will describe in more detail only the electronic structure of the n = 1+ molecule.

(66) Verdaguer, M.; Gleizes, A.; Renard, J. P.; Seiden, J. *Phys. Rev. B* **1984**, *29*, 5144.

(67) Kai, A. T.; Larsson, S. *Int. J. Quantum Chem.* **1978**, *13*, 367.

Group theory can help us in assigning bonding and antibonding character to the computed molecular orbitals. The valence orbitals belong to the following irreducible representations of D_{3d}:

atom	orbital	n	symmetry
Co	4s	6	$a_{1g} + e_g + a_{2u} + e_u$
	3d	30	$3a_{1g} + 2a_{2g} + 5e_g + 2a_{1u} + 3a_{2u} + 5e_u$
S	3p	24	$3a_{1g} + a_{2g} + 4e_g + a_{1u} + 3a_{2u} + 4e_u$
P	3s	6	$a_{1g} + e_g + a_{2u} + e_u$
	3p	18	$2a_{1g} + a_{2g} + 3e_g + a_{1u} + 2a_{2u} + 3_{eu}$
H	1s	18	$2a_{1g} + a_{2g} + 3e_g + a_{1u} + 2a_{2u} + 3e_u$

The orbitals of the PH_3 ligands available for bonding span the $a_{1g} + e_g + a_{2u} + e_u$ irreducible representations; we therefore expect 24 bonding Co–S orbitals and 6 bonding Co–P orbitals for a total of 30 bonding orbitals. Another 30 orbitals will be the antibonding counterparts. Six cobalt orbitals of symmetry $a_{2g} + e_g + a_{1u} + e_u$ will therefore be nonbonding, when only nearest neighbor interactions are considered.

According to the charge distribution on the molecule we can assign the orbitals between −20.4 and −19.0 eV to 3s orbitals of S, almost nonbonding. Above these orbitals, between −18.06 and −17.98 eV, there are the six 3s orbitals of P, involved in a bonding interaction with the hydrogens. Between −11.7 and −9.13 eV, we find a closely spaced set of energy levels, like a band, which can be defined as mixed metal–ligand bonding orbitals. There is no net energy separation between bonding metal–sulfur and metal–phosphorus interactions, indicating that both bonds contribute to the stability of the molecule with comparable strength. The set of 30 antibonding and 6 nonbonding orbitals form a band of energy levels spread out between −7.86 and −3.97 eV. The 6 almost nonbonding levels can be individuated between −7.86 and −7.66 eV as the levels with the largest charge on the cobalt sphere and small intersphere charge. The energy levels belonging to the antibonding band are separated by an energy gap of ≈1.8 eV which appears between the $12E_u$ (HOMO) and $13E_u$ (LUMO) orbitals. The origin of this HOMO-LUMO energy gap can be understood on looking at the charge distribution. The charge density on cobalt in the empty orbitals up to $13E_g$ is, in fact, around 55%, indicating rather strong covalency, and these orbitals have both P and S antibonding character. The orbitals with only P ($10A_{1g}$) or S ($12E_g$) antibonding character fall into the lowest part of the band.

In the above calculation we have implicitly assumed that the electronic configuration corresponding to the occupancy of the lowest energy levels represents the more stable configuration. Since we have a series of molecular levels very closely spaced in energy, a number of electronic configurations differing by one electron in the occupancy of one of these levels actually have very close total energies. Actually the $^2A_{2u}$ state, arising from the configuration $(...9A_{2u}^1\ 12E_u^4)$, is more stable than the ^2E_u state, coming from $(...9A_{2u}^2\ 12E_u^3)$, by ≈0.02 eV. Other doublet levels at energies lower than 0.3 eV exist. These doublet states form a series of levels that are the molecular orbital representation of the exchange split multiplets used in the interpretation of the EPR results. These doublet states could give rise to an efficient mechanism for electron relaxation[68] and can explain why the EPR spectra are unobservable at temperatures greater than ≈30 K even in dilute solutions whatever is the nature of the counterion. Apart from this uncertainty in the choice of the real ground configuration, which however is more relevant only for the quasidegenerate $12E_u$ and $9A_{2u}$ levels, exchange energy can also play a fundamental role in determining the ground-state configuration. When $n = 1$, for example, we also can have a high-spin configuration of the type $(12E_u^2\ 13E_u^1)$, leading to a quartet spin state, which can become the ground-state configuration if electron exchange is important. The total energy computed for this configuration, using spin unrestricted calculation, is largely above the total energy of the ground doublet, in agreement with the experimental finding, and, furthermore, spin restricted and spin unrestricted calculations on the quartet state give total energies which differ by only a small amount (<0.03 eV). This fact confirms that electron exchange does not give a significant contribution to the total energy of the cluster. Similar results were also obtained for $n = 2+$ and $2-$, and in the following we will report only the spin-restricted results.

(68) Abragam, A.; Bleaney, B. *Electron Paramagnetic Resonance of Transition Ions*; Oxford University Press: Oxford, UK, 1970.

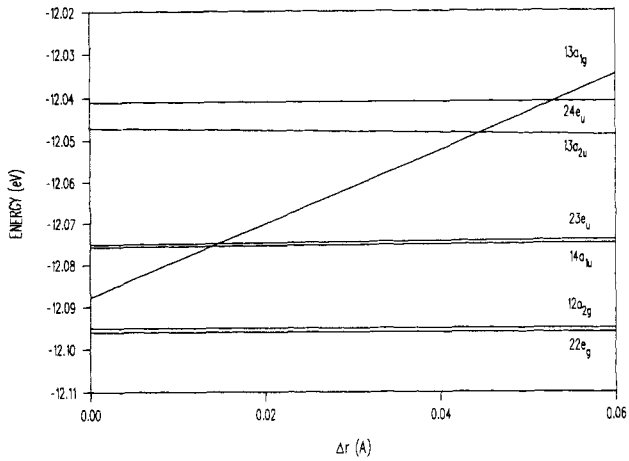

Figure 10. Variation of the energies of the HOMO and the next nearest occupied molecular orbitals as a function of $\Delta r = (2.161\ \text{Å} - r\ (\text{Å}))$ with r ranging from 2.161 to 2.101 Å. Extended Hückel results for the model compound $[Co_6(\mu_3\text{-}S)_8(PH_3)_6]^+$

As far as the nature of the ground state is concerned, it has to be observed here that the analysis of the g values gave $^2A_{1g}$ as the ground state, while the present calculations give $^2A_{2u}$. A reasonable explanation for this fact comes from extended Hückel calculations performed on varying the cobalt–phosphorus bond lengths. In Figure 10 the effect of changing the Co–P bond length from 2.16 to 2.10 Å on the energies of the HOMO and the next nearest occupied molecular orbitals is shown. The largest effect is experienced by the $13a_{1g}$ level ($10A_{1g}$ of the Xα-SW calculations) which has the largest phosphorus antibonding character. This level becomes the HOMO for a Co–P distance around 2.12 Å. It is evident that the exact nature of the ground state is very sensitive to small geometrical distortions and, therefore, that vibronic effects should be important in determining the electronic structure.[5] It is also apparent that molecular orbital calculations, which are based on a static configuration of the nuclei and generally require the use of some idealized geometry, cannot reproduce all the subtleties of the electronic structure of the present cluster in the temperature range of the experiments.

Another check of the quality of the present calculations for the description of the overall electronic structure of the cluster, except for the very-low-temperature range of the EPR experiments, comes from the calculations of the dipole-allowed electronic transition energies.[44] A graphical comparison between the computed transitions and the experimental spectrum is shown in Figure 3. The overall agreement with experiment is apparent. The computed transitions which arise from one-electron excitations from the levels between $10A_{1g}$ and $9E_g$ to the $9A_{2u}$ levels (we used the $^2A_{2u}$ electronic configuration in all these calculations) can be grouped into a low-energy region ranging almost continuously up to 1587 nm (6300 cm^{-1}) and into d–d and charge transfer (CT) transitions. Transitions labeled d–d are computed at 586 nm (17 070 cm^{-1}) ($9A_{2u} \rightarrow 13E_g$), 499 nm (20 050 cm^{-1}) ($9A_{2u} \rightarrow 11A_{1g}$), 494 nm (20 220 cm^{-1}) ($9A_{2u} \rightarrow 14E_g$), 401 nm (24 950 cm^{-1}) ($8A_{1g} \rightarrow 9A_{2u}$), and 390 nm (25 650 cm^{-1}) ($7A_{1g} \rightarrow 9A_{2u}$). Higher energy bands can be assigned to CT transitions from the orbitals $6A_{1g}$, $1A_{2g}$, $5E_g$, $5A_{1g}$, $4E_g$, $4A_{1g}$, $3E_g$, and $3A_{1g}$ to $9A_{2u}$. The computed energies are 339 nm (29 500 cm^{-1}), 298 nm (33 500 cm^{-1}), 294 nm (33 470 cm^{-1}), 294 nm (34 000 cm^{-1}), 291 nm (34 300 cm^{-1}), 288 nm (34 660 cm^{-1}), and 268 nm (37 300 cm^{-1}), respectively.

Upon adding one electron to $[Co_6(\mu_3\text{-}S)_8(PEt_3)_6]^+$ we obtain the $n = 0$ uncharged complex. The computed ground state has a configuration $(...12E_u^4)$, corresponding to a singlet diamagnetic ground state, as experimentally observed.[28]

MO calculations performed on a series of clusters should reproduce and explain the relative stability of the different com-

pounds and, eventually, predict those of new ones. The approximations involved in the SW procedure[39] prevent us from doing such an analysis, since the computed total energies are affected by the approximations of the method. In particular the use of the Watson sphere causes shifts of the one-electron levels, adding different contributions to the total energies. From general considerations, however, we learn that a large HOMO-LUMO gap is associated to chemical stability and we can infer that the rather large HOMO-LUMO energy gap, computed for the $n = 0$, 1+ clusters, should cause the negatively charged species to be at significantly higher energy with respect to the neutral and cationic species. This gives a theoretical justification to the fact that anionic clusters have not been observed electrochemically. On the same grounds we can expect a larger stability for the $n = 0$ and 1+ clusters as compared to the $n = 2+$ one, which should have small HOMO-LUMO gaps.

It has to be mentioned now that since geometry optimization is not meaningful in the SW approximation we are looking at a molecule with fixed geometry, and we can only say that the assumed geometry is not consistent with the given charge. A geometrical deformation could also in principle stabilize the higher energy states. The Hellmann–Feynman forces (HF) on cobalt, computed through eq 1, can give more information, since they reflect the minimization of the nuclear repulsion by the electronic cloud. Taking as zero force that computed for $n = 0$, we compute the following percent variations of the forces on the cobalt nuclei

n	ΔHF (%)
0	0
1+	−3.6
1−	+0.5
2+	−0.5
2−	+1

Only for the 1+ charged molecule is the electronic distribution computed to appreciably influence its stability, suggesting that some molecular deformation should also contribute to the stability of the 1+ charged molecule. As a matter of fact, differences were observed in the Co–Co distances for the $n = 0$ and 1+ clusters, being 2.817 (3) and 2.788 (1) Å, respectively.

Conclusions

The electronic structure of $[Co_6(\mu_3\text{-}S)_8(PEt_3)_6](PF_6)$ is characterized by one unpaired electron delocalized over the whole cluster. The electron delocalization generates a number of doublet states close to the ground state and gives efficient spin relaxation mechanisms which, shortening the electronic relaxation time, make the cluster EPR silent at room temperature, even in dilute solutions where the nature of the counterion, which can modulate solid-state interactions, has no influence. The axial **g** tensor at 4.2 K for $[Co_6(\mu_3\text{-}S)_8(PEt_3)_6](PF_6)$, which has a crystallographic $S_6 = C_3 \otimes i$ symmetry, was nicely reproduced using the localized **g** tensor seen in the EPR spectra of the triclinic complex $[Co_6(\mu_3\text{-}S)_8(PEt_3)_6](BPh_4)$. The axial symmetry and the principal g values arise naturally as a spatial average of single ion $\mathbf{g}_i$ tensors in agreement with a delocalization of the single unpaired electron on the whole cluster, required by the crystallographic symmetry.

It is important to stress that we are in the presence of a strong influence of the actual site symmetry of the cluster on the localization–delocalization of the unpaired electron. We offer this rationale as the simplest interpretation of the experimental data.

It is apparent that EPR spectroscopy shows some effects which cannot be observed on the scale of the magnetic measurements. Of course the interpretation of these data suffers of some approximation.

The cluster molecules are not magnetically isolated and, even if the presence of the axial PEt_3 ligands prevents the formation of spatially extended solids, like the Chevrel phases of the molibdenum chalcogenides, feeble ferromagnetic interactions between the clusters are experimentally measurable. Looking for molecular systems which could enhance the strength of this interaction is a possible development.

Xα-SW calculations have shown that the presence of the phosphine ligands in the axial positions adds an energy gap in the band formed by the cluster antibonding molecular orbitals. The effect of this energy gap is at first glance that of forcing a low-spin configuration of the whole molecule.

The exact ordering of the energy levels inside the band is extremely sensitive to small geometrical deformations such as variations in the Co–P bond length. Any theoretical calculations performed on these systems probably cannot reproduce all of the observed properties. A good agreement was obtained in reproducing the observed electronic transitions, while the ground state differs from that consistent with the 4.2 K EPR spectra.

A number of experimental facts have also been rationalized using this MO theory, namely, the observed diamagnetism of the uncharged cluster and the relative instability of negatively and positively charged species which should possess small HOMO-LUMO energy gaps. The calculated Hellmann–Feynman force on cobalt in the uncharged, $n = 0$, cluster, significantly different from that of the monocationic, $n = 1+$, cluster, rationalized the differences in Co–Co distance seen in the crystal structures and indicated that molecular deformations from the ideal structure, which can be responsible for the stabilization of positively charged species, should have the largest effect for the monocationic species.

Acknowledgment. Thanks are expressed to Prof. O. Kahn, Université de Paris Sud, for the magnetic measurements, to Prof. M. Verdaguer, Université P. et M. Curie, Paris, for the kind hospitality and helpful discussions, to Prof. Dante Gatteschi, Università di Firenze, for helpful suggestions, and to Mr. Franco Cecconi for the assistance in the chemical manipulations.

Supplementary Material Available: PLUTO packing diagram, tables of the calculated coordinates of the hydrogen atoms and of the final thermal parameters, table of the final atomic parameters of the non-hydrogen atoms, and table of nuclear coordinates and selected interatomic distances for the model compound $[Co_6(\mu_3\text{-}S)_8(PH_3)_6]^+$ (6 pages); table of observed and calculated structure factors (9 pages). Ordering information is given on any current masthead page.